Quantum dot microcavity control of photon statistics
Snijders, H.J.

Citation
Snijders, H. J. (2018, December 20). *Quantum dot microcavity control of photon statistics*. *Casimir PhD Series*. Retrieved from https://hdl.handle.net/1887/67538

Cover Page

Universiteit Leiden

The handle http://hdl.handle.net/1887/67538 holds various files of this Leiden University dissertation.

Author: Snijders, H.J.
Title: Quantum dot microcavity control of photon statistics
Issue Date: 2018-12-20

Chapter 3

Quantum master model for cavity QED

In this chapter, we describe the full quantum master model and show how it is solved numerically. We discuss the driven Jaynes–Cummings Hamiltonian in the semi-classical and quantum regime. Additionally, we explain how the full quantum master model is useful in simulating more complicated level structures such as exciton, biexciton and trion state.

Part of the content in this chapter is used in the publications of later chapters.

3.1 Quantum master equation

In order to fully understand the quantum behavior of a QD interacting with photons in a cavity, we solve the quantum master equation numerically. This allows us to include the quantum correlations between the photon operators and QD operators, and other relaxation mechanisms such as pure dephasing. Using the Hamiltonian of Eq. 2.15 and including a Lindblad-type of dissipation, the master equation becomes

$$\frac{d\rho}{dt} = \mathfrak{L}\rho = -i\left[\hat{H}, \rho\right] + 2\kappa\mathfrak{D}\left[\hat{a}\right]\rho + \gamma_{\|}\mathfrak{D}\left[\hat{S}_-\right]\rho + \frac{\gamma^*}{2}\mathfrak{D}\left[\hat{S}_z\right]\rho. \tag{3.1}$$

Here, compared to Eq. 2.16, we have included a term that describes the pure dephasing γ^*. Pure dephasing conserves the population of the excited and ground states, but effects the coherence of the transition since it modifies the off-diagonal terms in the density matrix ρ. This Lindblad-type master equation in Eq. 3.1 is based on several additional assumptions (see for instance [37]). Here we point out the three most important ones. (1) Full separability of the system and the environment at $t = 0$. (2) The state of the environment must not change significantly under interaction with the system, i.e., the interaction is weak, and the system and environment remain separable throughout the evolution. (3) The environment has no memory on the time scale of the evolution (Markov approximation).

3.1.1 Steady-state solution

For the steady-state solution, with continuous wave excitation, we solve $\mathfrak{L}\rho = 0$ using the numerical methods provided by the software package QuTiP [38]. The density matrix ρ of the steady-state solution is the tensor product of the QD-system matrix with the photon density matrix. In order to obtain the steady-state solution, the time-dependence in the Hamiltonian needs to be removed. This is done by transforming the Hamiltonian to the Heisenberg picture, but in order to do this transformation the fast rotating terms in the time-dependence are removed by using the rotating wave approximation. To apply the rotating wave approximation two conditions need to be satisfied: $f_{cav} \approx f_a$, and $f_a \gg \Omega$. Here f_{cav} is the cavity frequency, f_a is the QD transitions frequency and Ω is the Rabi frequency. Figure 3.1 shows that, in the weak coupling regime, the rotating wave approximation is valid for a broad range of input powers. In the regime of ultra-strong coupling, the rotating wave approximation breaks down [39].

3.1.2 Time-dependent solution

In case the time-dependence cannot be removed from the Hamiltonian, the quantum master equation can be solved as a function of time. In Qutip, there are three methods to find time-dependent expectation values: a direct method, an exponential series expansion and a Monte Carlo simulation. The direct method uses a matrix evolution and solves the system iteratively with time steps τ, where τ is considered to be small. In the exponential series expansion, the solution for the expectation value of the cavity field is written as [38]

$$\left\langle \hat{a}^\dagger(\tau)\hat{a}(0)\right\rangle = Tr\left(\hat{a}^\dagger e^{[\mathfrak{L}]t}\hat{a}\rho_0\right) = Tr_{(i)}\left(\sum \varphi_k^{(i)}\exp\left(-s_k\left|\tau\right|\right)\right), \tag{3.2}$$
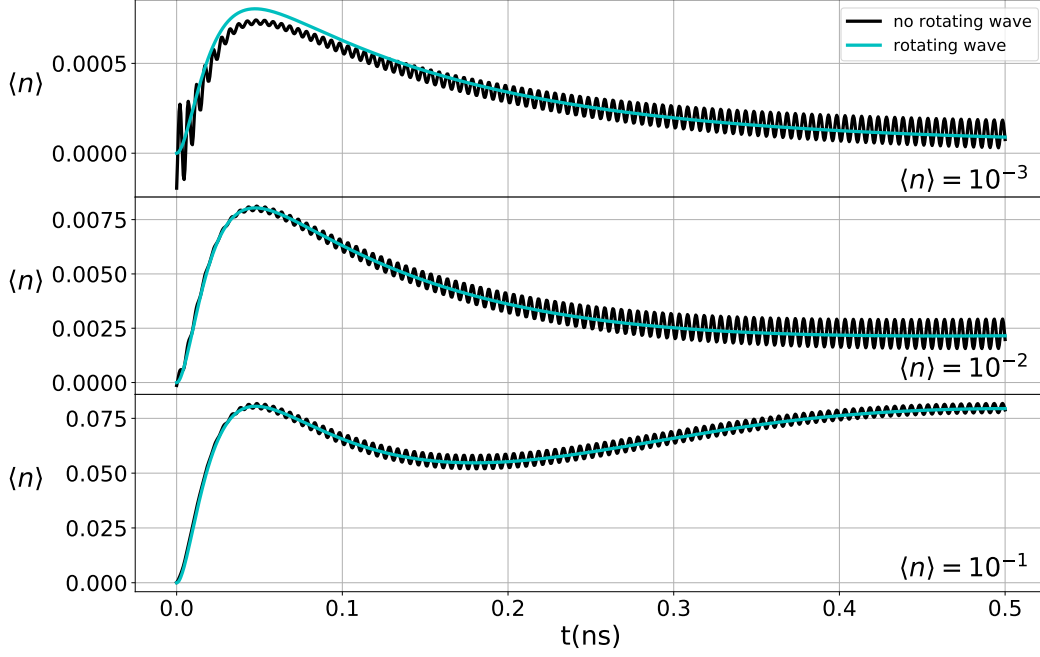
Figure 3.1: Comparison of the Hamiltonian with and without rotating wave approximation for different driving powers.

where s_k are the eigenvalues of $\mathfrak{L}$ and φ_k are the amplitude coefficients. In most cases, the direct method is fastest, only for extremely long evaluation times of the system or large density matrices it is favorable to use a Monte Carlo simulation.

3.1.3 Spectral distribution of the emitted light

The frequency spectrum of the emitted light is found by taking the Laplace transform of $\left\langle \hat{a}^\dagger(\tau)\hat{a}(0) \right\rangle$. This, however, only gives the correct frequency spectrum if the spectrum is completely symmetric around zero frequency. Calculating the Fourier transform of an expectation value gives the frequency spectrum

$$S(\omega) = \int_{-\infty}^{\infty} \left\langle \hat{a}^\dagger(\tau)\hat{a}(0) \right\rangle e^{i\omega\tau} d\tau. \tag{3.3}$$

This equation can be solved using a fast Fourier transform if the solution of the expectation value is provided using matrix evolution. However, when the solution is provided using an exponential series expansion, a nice trick becomes available to calculate the frequency spectrum. Using the exponential series expansion we can write

$$S(\omega) = \int_{-\infty}^{\infty} \left\langle \hat{a}^\dagger(\tau)\hat{a}(0) \right\rangle e^{i\omega\tau} d\tau = \int_{-\infty}^{\infty} \sum_k \varphi_k^{(i)} \exp\left(-s_k |\tau|\right) e^{i\omega\tau} d\tau. \tag{3.4}$$

Exchanging the integral and the summation, this can be rewritten as

$$S(\omega) = \sum_k \int_{-\infty}^{\infty} \varphi_k \exp\left(-s_k |\tau|\right) e^{i\omega\tau} d\tau = 2Re \sum_k \frac{\varphi_k}{i\omega - s_k}. \tag{3.5}$$

This shows that the exponential series expansion almost directly gives the frequency spectrum of the transmitted light.

3.2 Comparison of the quantum master equation with semi-classical models

In semi-classical models QD-Electromagnetic field correlations are not taken into account. Therefore, comparing the cavity transmission obtained via a numerical simulation of the quantum master equation with results from semi-classical calculations provides insight in how QD-field correlations affect the system. The numerical simulation grants us access to the density matrix, which contains all the system information such as quantum correlations and the coherence functions. In Fig. 3.2, we compare the cavity transmission as a function of laser frequency for the classical case described by Eq. 2.19 and respresented by the dashed lines, to the numerically obtained quantum case described by Eq. 3.1 and represented by the solid lines. The transmission is given in terms of the cavity mean photon number $\langle n \rangle$. A limitation of the numerical simulation is that the density matrix size grows exponentially with the photon number (and QD states). Here, the density matrix contains Fock states up to 10 photons, which is sufficient for a mean photon number of 10^{-1} or lower.
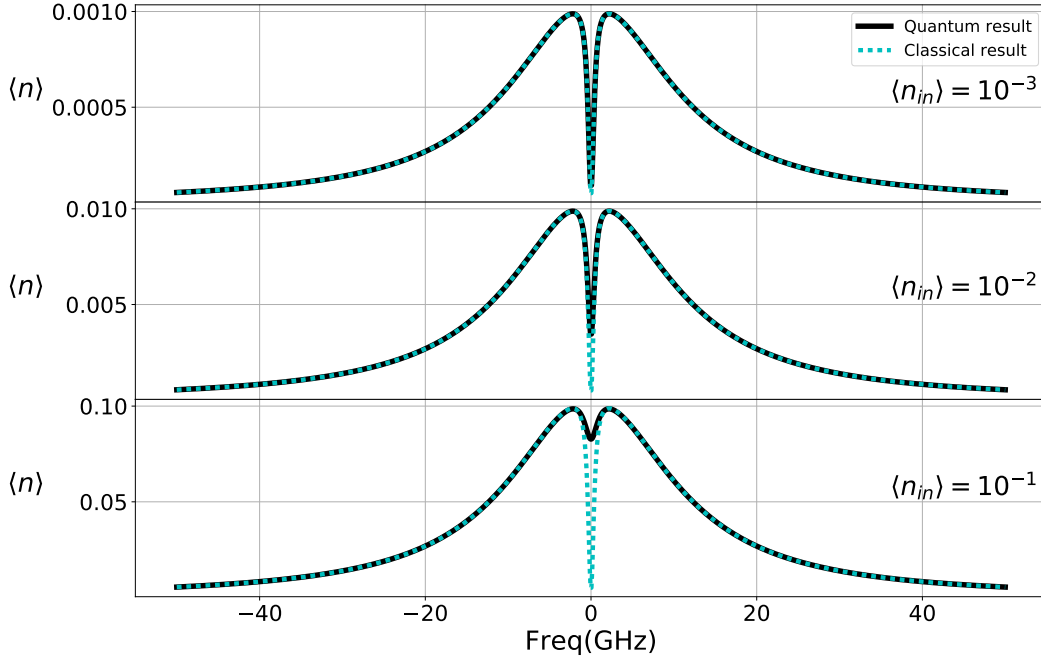
Figure 3.2: Transmission of a QD transition in resonance with a cavity as a function of the laser frequency. The simulation is carried out for three different mean photon numbers $\langle n_{in} \rangle = 10^{-1}$, 10^{-2}, 10^{-3} in the cavity. Increasing the power shows saturation of the QD transmission dip when using a numerical simulation of the quantum master equation (solid line), while for the classical case (dashed line), this is not reproduced. Other parameter values are: $\kappa = 12\,\text{GHz}$, $\gamma_{\parallel} = \frac{1}{2\pi}\,\text{GHz}$, $\gamma^* = 0\,\text{GHz}$ and $g = 2\,\text{GHz}$.

When the quantum master equation is solved numerically, we observe a saturation response of the transmission dip for increasing input power, proportional to $\langle n_{in} \rangle$. Here, $\langle n_{in} \rangle$ is the mean photon number in the cavity. This saturation is not reproduced in the semi-classical calculation, since it is only valid in the low-excitation regime. Below $\langle n_{in} \rangle \approx 10^{-3}$, the quantum result and semi-classical result overlap, while increasing the power to $\langle n_{in} \rangle \approx 10^{-1}$ saturates the QD transition almost completely.

In order to study this dip depth in more detail, the relative dip depth is plotted in Fig. 3.3 as a function of input power. The relative dip depth is defined as $(\langle n \rangle - \langle n_{QD} \rangle) / \langle n \rangle$, where $\langle n_{QD} \rangle$ is the mean photon number in a cavity with a QD on resonance at a certain input power. For the semi-classical case, or for the case of a very low mean photon number, the relative dip depth is defined as

$$1 - \left(\frac{1}{1 + C} \right)^2,$$

where $C = \frac{g^2}{\kappa \gamma_{\perp}}$ is the cooperativity of the system. While in the semi-classical case, the relative dip depth does not change as a function of input power, we observe that, in the quantum case, the relative dip depth vanishes when increasing the power two-orders of magnitude from $\langle n_{in} \rangle = 10^{-3}$ to $\langle n_{in} \rangle = 10^{-1}$. In addition to the semi-classical and quantum results, the nonlinear semi-classical case (blue line in Fig. 3.3) is also plotted to
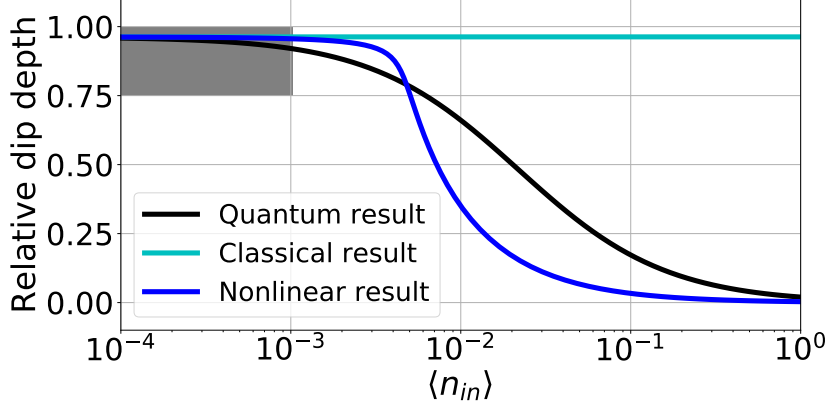
Figure 3.3: Relative dip depth as a function of the mean photon number. The results are plotted for the semi-classical case (Eq. 2.19), nonlinear semi-classical case (Eq. 2.49) and quantum case (Eq. 3.1), with parameter values $\kappa = 12$ GHz, $\gamma_{||} = \frac{1}{2\pi}$ GHz, $\gamma^* = 0$ GHz and $g = 2$ GHz. The grey box indicates the area where the power is low enough so that the classical and quantum results overlap.

show the effect of saturation in this model. Comparing the nonlinear classical case to the quantum case we observe that at low power, $\langle n_{in} \rangle \lesssim 10^{-3}$, and high power, $\langle n_{in} \rangle \gtrsim 1$, the results become nearly identical. This shows that quantum correlations are important for a mean photon number above $\langle n_{in} \rangle = 10^{-3}$.

Another important effect to discuss is pure dephasing, which is a non-radiative effect that effects the coherence of the QD transition. If significant pure dephasing is included, the relative dip depth at low mean photon number reduces, since pure dephasing destroys the coherence of the light in the cavity. In Fig. 3.4 (a), we plot the relative dip depth for the case with pure dephasing and observe that, for a pure dephasing of $\gamma^* = \frac{1}{2\pi}$ GHz, the dip depth decreases from ~ 1 to ~ 0.8 at an input mean photon number of $\langle n_{in} \rangle \sim 10^{-4}$. The other system parameters are similar to the simulation in Fig. 3.3. For the classical case, the pure dephasing is artificially inserted by defining $\gamma_\perp = \frac{\gamma_{||}}{2} + \gamma^*$. In order to characterize the effect of pure dephasing further, the relative dip depth is plotted in Fig. 3.4(b) as a function of the ratio $\left(\frac{\gamma^*}{\gamma_{||}}\right)$. From this we find, as indicated by the grey box in Fig. 3.4(b), if $\gamma^* \lesssim 0.1\gamma_{||}$, the effect of pure dephasing can safely be neglected. It also shows that, in the classical case for an input power of $\langle n_{in} \rangle \gtrsim 0.5$, the artificially inserted pure dephasing is not sufficient to describe the pure dephasing in the quantum model.

3.3 Quantum master simulations for quantum dot cavity QED

Here we explain in detail the structure of the quantum master equation for three types of excitations in QDs: neutral exciton, biexciton and trion. Furthermore, we derive a time-independent Jaynes–Cummings Hamiltonian which is then used to formulate the quantum master equation for each level structure. We argue that, for more involved level systems, a classical description is not sufficient and a full quantum master equation is
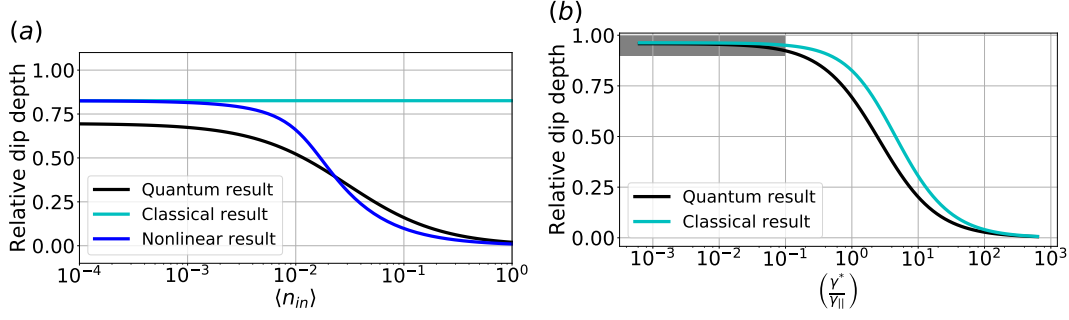
Figure 3.4: a) Relative dip depth as a function of the input power in the case with pure dephasing. The results are plotted for the classical case (Eq. 2.19), nonlinear classical case (Eq. 2.49) and quantum case (Eq. 3.1) with parameter values $\kappa = 12$ GHz, $\gamma_\parallel = \frac{1}{2\pi}$ GHz, $\gamma^* = \frac{1}{2\pi}$ GHz and $g = 2$ GHz. b) Relative dip depth as a function of pure dephasing γ^* with ($\langle n \rangle_{in} = 10^{-4}$). The grey box indicates the area where the effect of pure dephasing can be neglected.

necessary. Additionally, we discuss the effect of a magnetic field to briefly touch upon spin pumping effects that can take place in charged QDs.

3.3.1 Neutral exciton

In this section, a detailed analysis is given of the neutral exciton and the related optical transitions. We use a matrix formalism [33, 40], instead of the alternative method in terms of wave functions [41]. The geometry of the QD leads to the appearance of the fine-structure split transitions. They arise due to the exchange interaction which couples the spins of the electron and hole. In Fig. 3.5, we show the level structure of the neutral exciton as a result of the exchange interaction. The general form of the spin Hamiltonian for the electron-hole exchange interaction of an neutral exciton, formed by a hole spin J_h and by an electron with spin S_e, is given by [42]

$$H_{exchange} = - \sum_{i=x,y,z} \left(a_i J_{h,i} \cdot S_{e,i} + b_i J_{h,i}^3 \cdot S_{e,i} \right), \tag{3.6}$$

where a and b are the spin-spin coupling constants. Due to strain in self-assembled QDs, the heavy and light hole states are split in energy by several meV [40]. This splitting is considerably larger than the involved linewidths and the fine-structure interaction energy, and therefore, the light hole states can be neglected. The basis from which the neutral exciton is constructed therefore consist of a heavy hole with $J_h = 3/2$, $J_{h,z} = \pm 3/2$ and the electron $S_e = 1/2$, $S_{e,z} = \pm 1/2$. From these states four excitons are formed, which are characterized by their angular momentum projections $M = S_{e,z} + J_{h,z}$. Due to the optical selection rules, the $|M| = 2$ transitions cannot couple to the light field, and are therefore optically inactive (dark transitions), while the states with $|M| = 1$ are allowed

Neutral exciton

$$|e_l\rangle = \tfrac{1}{\sqrt{2}}(|\Uparrow\downarrow\rangle - |\Downarrow\uparrow\rangle) \qquad\qquad |e_r\rangle = \tfrac{1}{\sqrt{2}}(|\Uparrow\downarrow\rangle + |\Downarrow\uparrow\rangle)$$
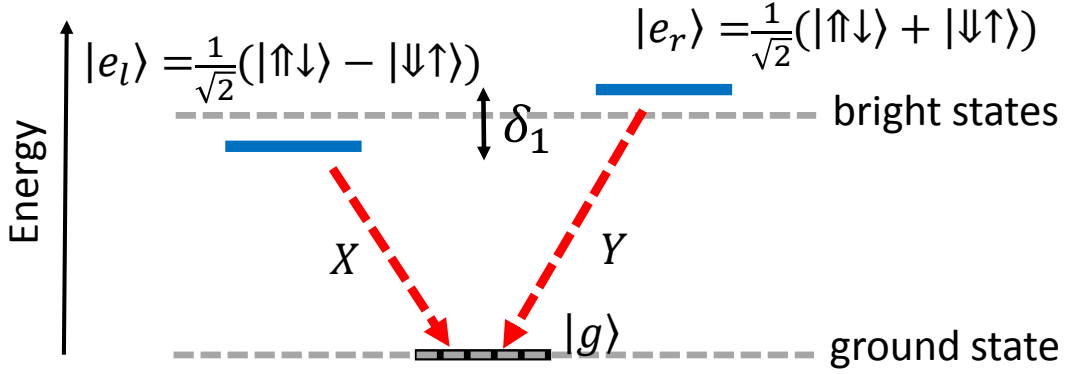
Figure 3.5: *Energy structure of an exciton. Due to symmetry breaking, the excited states are described as a superposition of $|\Uparrow\downarrow\rangle$ and $|\uparrow\Downarrow\rangle$, where up describes an electron, and doubleup a hole with spin up.*

(bright transitions). Using the exciton states

$$
\begin{aligned}
|+1\rangle &= |\Uparrow\downarrow\rangle \\
|-1\rangle &= |\Downarrow\uparrow\rangle \\
|+2\rangle &= |\Uparrow\uparrow\rangle \\
|-2\rangle &= |\Downarrow\downarrow\rangle
\end{aligned}
\tag{3.7}
$$

as a basis the following matrix representation is obtained

$$
H_{exchange} = \frac{1}{2}
\begin{pmatrix}
\delta_0 & \delta_1 & 0 & 0 \\
\delta_1 & \delta_0 & 0 & 0 \\
0 & 0 & -\delta_0 & \delta_2 \\
0 & 0 & \delta_2 & -\delta_0
\end{pmatrix},
\tag{3.8}
$$

where $\delta_0 = -3/4(a_z \tfrac{9}{4} b_z)$, $\delta_1 = 3/8(b_x - b_y)$, and $\delta_2 = 3/8(b_x + b_y)$. If we have a special neutral exciton under study with rotational symmetry (meaning that $b_x - b_y = 0$), then the angular momentum is still a good quantum number and $|+1\rangle$ and $|-1\rangle$ are degenerate eigenstates of $H_{exchange}$. On the other hand, when the rotational symmetry is broken ($b_x - b_y \neq 0$), the angular momentum is not a good quantum number anymore and the eigenstates are transformed in the linear polarized states $\frac{1}{\sqrt{2}}(|\Uparrow\downarrow\rangle + |\uparrow\Downarrow\rangle)$, $\frac{1}{\sqrt{2}}(|\Uparrow\downarrow\rangle - |\uparrow\Downarrow\rangle)$. This situation is sketched in Fig. 3.5. In practice, we encounter nearly always an exciton with a broken symmetry so that the observed spectrum has two excitation peaks.

Neutral exciton with external magnetic field

An exciton in a magnetic field experiences a Zeeman splitting of the energy levels. The general interaction of the electron and hole spins with an external magnetic field B is given by
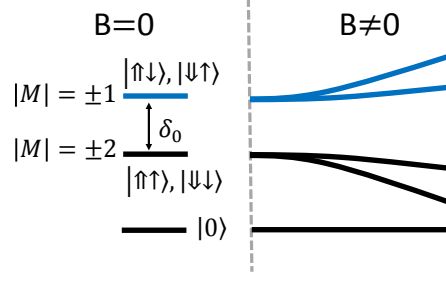
Figure 3.6: Zeeman splitting for the bright $|M| = \pm 1$ and dark $|M| = \pm 2$ transitions in Voigt configuration. Mixing of the eigenstates makes the dark transitions become visible.

$$H_{zeeman} = \mu_B \sum_{i=x,y,z} (g_{e,i} S_{e,i} + \frac{g_{h,i}}{3} J_{h,i}) B_i, \qquad (3.9)$$

where μ_B is the Bohr magneton, and g_e and g_h are the Landé g-factors for the electron and hole. In general, there are two popular magnetic field geometries, the Faraday geometry, in which the magnetic field is applied parallel to the growth direction of the heterostructure, or the Voigt geometry, in which case it is in-plane. In the Faraday geometry, for strong enough magnetic fields, the states of Eq. 3.7 become again eigenstates of the system and the emitted light is completely circularly polarized. In the Voigt geometry, the in-plane magnetic field destroys the rotational symmetry and also causes mixing of bright and dark excitons, resulting in the observation of 4 lines in the QD spectrum. The matrix representation of this Hamiltonian for a magnetic field aligned in the x-direction is given as

$$H_{exchange} + H_{Zeeman} = \frac{1}{2} \begin{pmatrix} \delta_0 & \delta_1 & \mu_B B g_{e,x} & \mu_B B g_{h,x} \\ \delta_1 & \delta_0 & \mu_B B g_{h,x} & \mu_B B g_{e,x} \\ \mu_B B g_{e,x} & \mu_B B g_{h,x} & -\delta_0 & \delta_2 \\ \mu_B B g_{h,x} & \mu_B B g_{e,x} & \delta_2 & -\delta_0 \end{pmatrix}, \qquad (3.10)$$

where the matrix is written down in the basis given by the states in Eq. 3.7. The eigenstates of this matrix show that $|M| = \pm 1$ and $|M| = \pm 2$ states mix when a magnetic field is applied, making the dark state transitions visible. The dark states become typically visible at around $B = 2\,T$ [43]; here this depends on the growth conditions of the QD. The sketch in Fig. 3.6 shows the influence of a magnetic field on the exciton levels. For clarity, we assume here a perfect symmetric neutral exciton meaning that $\delta_1 \approx \delta_2 \approx 0$, and observe the well-known splitting into 4 energy levels by increasing the magnetic field.

Quantum master equation for a neutral exciton

Here, we explain how the Jaynes–Cummings Hamiltonian for a system with a single two-level system can be modified to describe a neutral exciton in a QD. A neutral exciton can be described by a V-system, with two excited states and one ground state. These three

levels are written as

$$|g\rangle = \begin{pmatrix} 1 \\ 0 \\ 0 \end{pmatrix} \quad |e_l\rangle = \begin{pmatrix} 0 \\ 1 \\ 0 \end{pmatrix} \quad |e_r\rangle = \begin{pmatrix} 0 \\ 0 \\ 1 \end{pmatrix}. \quad (3.11)$$

In this case we obtain two instead of one raising operators

$$S_{l+} = |e_l\rangle\langle g| \quad S_{r+} = |e_r\rangle\langle g|. \quad (3.12)$$

The Jaynes–Cummings Hamiltonian now becomes

$$H = (\omega_c - \omega_p)\,\hat{a}^\dagger\hat{a} + (\omega_l - \omega_p)\,\hat{S}_{l+}\hat{S}_{l-} + g\left(\hat{S}_{l-}\hat{a}^\dagger + \hat{S}_{l+}\hat{a}\right) + (\omega_r - \omega_p)\,\hat{S}_{r+}\hat{S}_{r-}$$
$$+ g\left(\hat{S}_{r-}\hat{a}^\dagger + \hat{S}_{r+}\hat{a}\right) + \eta\left(\hat{a} + \hat{a}^\dagger\right). \quad (3.13)$$

Inserting this Hamiltonian into the quantum master equation gives

$$\frac{d\rho}{dt} = \mathfrak{L}\rho = -i\left[\hat{H}, \rho\right]$$
$$+ 2\kappa\mathfrak{D}\left[\hat{a}\right]\rho + \gamma_{||}\mathfrak{D}\left[\hat{S}_{l-}\right]\rho + \gamma_{||}\mathfrak{D}\left[\hat{S}_{r-}\right]\rho + \frac{\gamma^*}{2}\mathfrak{D}\left[\hat{S}_{rz}\right]\rho + \frac{\gamma^*}{2}\mathfrak{D}\left[\hat{S}_{rz}\right]\rho, \quad (3.14)$$

where we assume that the QD-cavity coupling constant g, as well as $\gamma_{||}$ and γ^* are equal for both exciton transitions. Increasing the number of transitions is a straightforward extension. Having N transitions with each their own resonance frequency, the Hamiltonian of Eq. 2.15 becomes

$$H = (\omega_c - \omega_p)\,\hat{a}^\dagger\hat{a} + \sum_{i=0}^{N}(\omega_i - \omega_p)\left(\hat{S}_+\right)_i\left(\hat{S}_-\right)_i + \sum_{i=0}^{N} g_i\left(\left(\hat{S}_-\right)_i\hat{a}^\dagger + \left(\hat{S}_+\right)_i\hat{a}\right) + \eta\left(\hat{a} + \hat{a}^\dagger\right). \quad (3.15)$$

The quantum master equation can still be solved in exactly the same manner as with a single transition. We can go a step further and also assume M cavity modes, which leads to the Hamiltonian

$$H = \sum_{i=0}^{N}(\omega_i - \omega_p)\left(\hat{S}_+\right)_i\left(\hat{S}_-\right)_i$$
$$+ \sum_{j=0}^{M}\left((\omega_j - \omega_p)\,\hat{a}_j^\dagger\hat{a}_j + \sum_{i=0}^{N} g_i\left(\left(\hat{S}_-\right)_i\hat{a}_j^\dagger + \left(\hat{S}_+\right)_i\hat{a}_j\right) + \eta_j\left(\hat{a}_j + \hat{a}_j^\dagger\right)\right). \quad (3.16)$$

Numerically, this Hamiltonian can still be solved as long as the density matrix becomes not extremely large. In practice, finding solutions with $N < 20$ photons is feasible with moderate memory requirements (16 GB of RAM). This condition is used throughout the entire thesis.

3.3.2 Biexciton

The biexciton consists of two electrons and two holes. The level structure of a biexciton, shown in Fig. 3.7, is related to an exciton, because the biexciton turns into an exciton after the first electron-hole recombination. When applying a magnetic field in Faraday
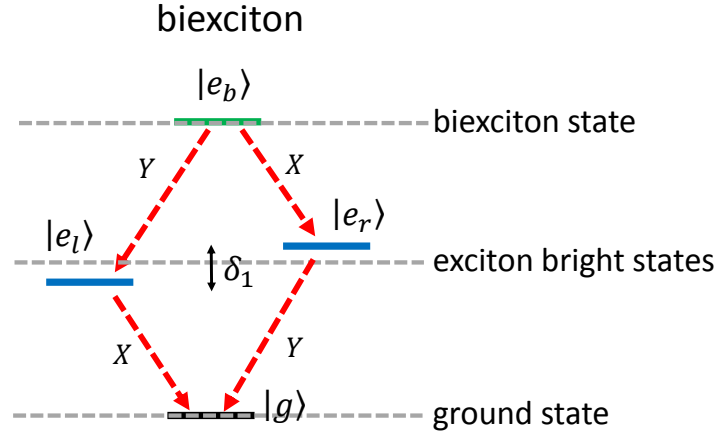
Figure 3.7: Level structure of a biexciton. After the first electron-hole recombination, a normal exciton remains.

configuration, the emitted light will change polarization from linear to circular for both the exciton and biexciton. In order to distinguish those, excitation power dependent intensity measurements can reveal the quadratic dependence of the biexciton transition [44].

The Jaynes–Cummings Hamiltonian for biexcitons can be derived easily but there are some strings attached to it. Using the basis

$$
|g\rangle = \begin{pmatrix} 1 \\ 0 \\ 0 \\ 0 \\ 0 \end{pmatrix} \quad |e_l\rangle = \begin{pmatrix} 0 \\ 1 \\ 0 \\ 0 \\ 0 \end{pmatrix} \quad |e_r\rangle = \begin{pmatrix} 0 \\ 0 \\ 1 \\ 0 \\ 0 \end{pmatrix} \quad |e_{b1}\rangle = \begin{pmatrix} 0 \\ 0 \\ 0 \\ 1 \\ 0 \end{pmatrix} \quad |e_{b2}\rangle = \begin{pmatrix} 0 \\ 0 \\ 0 \\ 0 \\ 1 \end{pmatrix} \quad (3.17)
$$

the raising operators become

$$
(S_+)_0 = |e_l\rangle \langle g| \quad (S_+)_1 = |e_r\rangle \langle g| \quad (S_+)_2 = |e_{b1}\rangle \langle e_l| \quad (S_+)_3 = |e_{b2}\rangle \langle e_r|, \quad (3.18)
$$

as do their corresponding lowering operators. A 5-dimensional basis is used where the states $|e_{b1}\rangle$ and $|e_{b2}\rangle$ each contain two electrons. Using these operators, one can construct the Hamiltonian

$$
H = (\omega_c - \omega_p)\, \hat{a}^\dagger \hat{a} + \sum_{i=0}^{3} (\omega_i - \omega_p) \left(\hat{S}_+\right)_i \left(\hat{S}_-\right)_i + \sum_{i=0}^{3} g_i \left(\left(\hat{S}_-\right)_i \hat{a}^\dagger + \left(\hat{S}_+\right)_i \hat{a}\right) + \eta \left(\hat{a} + \hat{a}^\dagger\right),
$$
(3.19)

where ω_i is the resonance frequency for the i-th transition of the biexciton. There is, however, one property of the biexciton that is not considered. If one electron is in the state $|e_b\rangle$, it can decay via two pathways, but in the formalism, this is fixed to one of the pathways based on the $|(S_-)_1\rangle$ or $|(S_-)_2\rangle$ lowering operator. The problem is that
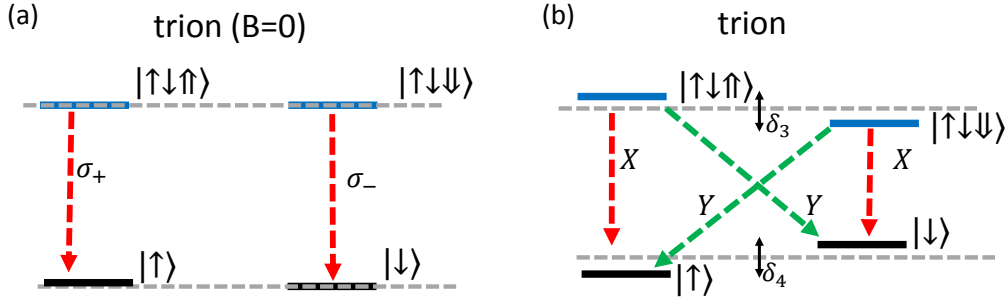
Figure 3.8: (a) Charged exciton without an magnetic field and (b) a charged exciton with a magnetic field. δ_2, δ_3 are the splittings between the different spin levels as a result of the Zeeman effect. $\{\sigma_+, \sigma_-\}$ represents the circular polarization basis and $\{X, Y\}$ the linear polarization basis.

one wants $|e_{b1}\rangle$ and $|e_{b2}\rangle$ to be orthogonal, but, at the same time, have a connection to each other. For the emission spectrum of the biexciton, it is often sufficient to insert the Hamiltonian of Eq. 3.19 into the quantum master equation. The obtained quantum master equation is similar to that of the exciton (Eq. 3.14), but with the inclusion of the extra transitions and Lindblad dissipation operators.

3.3.3 Singly charged exciton

For the singly charged exciton, or trion, the QD contains permanently one electron together with an optically excited exciton, one obtains a four-level system. There are two single electron ground states (spin-up and spin-down) and two excited trion states. Since the hole spin relaxation is much faster than the electron spin relaxation (without magnetic field), we can simplify the four level trion structure (Fig. 3.8(a)) to a 3-level Λ system [45]. The resident electron spin is useful for quantum information applications such as quantum memories [46, 47].

We can distinguish between a trion and a neutral exciton experimentally, using the fact that the trion has a circular polarization basis and the exciton a linear polarization basis. Applying a magnetic field in the x-direction leads to a Zeeman shift of the energy levels, breaks the circular symmetry of the QD system and results in a linear polarization basis, see Fig. 3.8(b).

Using the lifted ground-state degeneracy of the trion due to a (external) magnetic field, one can prepare the spins in either the $|\uparrow\rangle$ or $|\downarrow\rangle$ by driving certain transitions with a laser. First experimental results of spin pumping where presented in [48] for a magnetic field in Faraday configuration and [45] for a magnetic field in Voigt configuration. Figure 3.9 shows a sketch of the interaction where there are in total 4 optical transitions possible in a linear polarization basis. In addition to these four optical transitions, there are also two spin-flip transitions, one for the electron spin Γ_{el} and one for the hole spin Γ_{hole}. The relaxation time of the electron spin is typically around $\frac{1}{\Gamma_{el}} = 1$ μs [49, 50], while the optical transitions lifetimes are around 1 ns. This means that, driving the $1X$ transition (Fig. 3.9) with a laser continuously, will eventually initialize the spin in the $|\downarrow\rangle$ state. This process is called spin pumping. Similar to a negatively charged exciton, there also exists a positively charged exciton. Here, even longer relaxation times for the hole spin
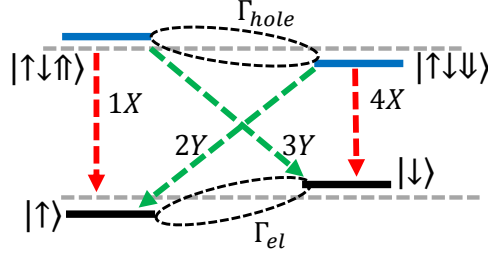
Figure 3.9: Schematic of a trion including the electron-spin (Γ_{el}) and hole-spin (Γ_{hole}) relaxation times.

can be obtained compared to the relaxation time for the electron spin in a negatively charged exciton [51].

3.3.4 Quantum master equation for a Λ system

For the three-level Λ system, we consider the ground states $|\uparrow\rangle$, $|\downarrow\rangle$ and the excited state $|e\rangle = |\uparrow\downarrow\Uparrow\rangle$ in Fig. 3.9. An important difference between a Λ system and a V-level system is the electron number conservation. The electron number conservation for a V-level system consist of two equations

$$\hat{P}_{el} = |e_l\rangle \langle e_l| + |g\rangle \langle g| = 1, \tag{3.20}$$

$$\hat{P}_{er} = |e_r\rangle \langle e_r| + |g\rangle \langle g| = 1. \tag{3.21}$$

These relations also follow the commutation relation of Eq. 2.13 and one can transform the time-dependent Hamiltonian into a time-independent one. For the Λ-system, the electron number conservation becomes

$$\hat{P}_{el} = |e\rangle \langle e| + |\uparrow\rangle \langle\uparrow| + |\downarrow\rangle \langle\downarrow| = 1. \tag{3.22}$$

In this case, it becomes much harder to find a unitary transformation to transform the Hamiltonian in a time-independent form and one is forced to resort to another approximation. The full Hamiltonian for a Λ system and a single cavity mode reads

$$H = \omega_c \hat{a}^\dagger \hat{a} + \omega_\uparrow |e\rangle \langle e| + \omega_\downarrow |\downarrow\rangle \langle\downarrow| + g\left(\hat{S}_- \hat{a}^\dagger + \hat{S}_+ \hat{a}\right) + \Omega\left(\hat{N}_- + \hat{N}_+\right) + \eta e^{i\omega_p}\left(\hat{a} + \hat{a}^\dagger\right), \tag{3.23}$$

where the raising operators are defined as $\hat{S}_+ = |e\rangle \langle\uparrow|$ and $\hat{N}_+ = |e\rangle \langle\downarrow|$, and Ω is the Rabi frequency for the transition from $|\downarrow\rangle$ to the $|\uparrow\downarrow\Uparrow\rangle$ state. Typically, this Hamiltonian is solved by transforming the system to the Heisenberg picture. This approach has the advantage that the time-dependence is removed from the density matrix of the system and canceled out against the time-dependent parts in the Hamiltonian and makes it mathematically and numerically easier to solve the system. Here, the trick to remove the time-dependence does not work since the unitary transformation $U =$

$e^{-it\left(\omega_p \hat{a}^\dagger \hat{a} + \omega_p \hat{S}_+ \hat{S}_- + \omega_p \hat{N}_+ \hat{N}_-\right)}$ does not remove all time dependent parts in the Hamiltonian 3.23. This leaves a time-dependence in the Ω term. In order to circumvent this problem, a more general unitary transformation $U = e^{-it\left(\omega_x \hat{a}^\dagger \hat{a} + \omega_y \hat{S}_+ \hat{S}_- + \omega_z \hat{N}_+ \hat{N}_-\right)}$ is used and we look for the conditions on $\omega_x, \omega_y, \omega_z$ that remove the time-dependence in the Hamiltonian [52]. To find stable solutions, the excited state $|e\rangle$ is adiabatically eliminated [53], which is allowed, since the lifetime of the excited state is much shorter compared to the relaxation time of the ground-state spin. Following these steps, the Hamiltonian can be written as

$$H = \left(\Delta_{cav} - \frac{g^2}{2\Delta_\uparrow}\right) \hat{a}^\dagger \hat{a} + \left(\Delta_\downarrow - \frac{\Omega^2}{2\Delta} - \frac{g^2}{\Delta_\uparrow}\hat{a}^\dagger \hat{a}\right) \hat{S}_z + \frac{g\Omega}{2\Delta_\uparrow}\left(\hat{S}_- \hat{a}^\dagger + \hat{S}_+ \hat{a}\right) + \eta\left(\hat{a} + \hat{a}^\dagger\right),$$
(3.24)

with $\Delta_{cav} = \omega_c - \omega_p$, $\Delta_\uparrow = \omega_\uparrow - \omega_p$, $\Delta_\downarrow = \omega_\downarrow - \omega_p$. This Hamiltonian has the extra term, proportional to $\sim \hat{a}^\dagger \hat{a} \hat{S}_z$ compared to the Hamiltonian for a V-level system. This extra term describes the interaction between the two ground states. This interaction becomes stronger if the mean photon number is higher or if the population of the excited state is higher. This Hamiltonian is only valid for the specific laser frequency ω_p, where the laser frequency ω_p drives the $|\uparrow\rangle$ to the $|\uparrow\downarrow\Uparrow\rangle$ state. To finalize the quantum master equation for a trion, we take into account the electron and hole spin relaxation rates. The quantum master equation becomes

$$\frac{d\rho}{dt} = \mathfrak{L}\rho = -i\left[\hat{H}, \rho\right] + 2\kappa \mathfrak{D}\left[\hat{a}\right]\rho + \gamma_{\parallel}\mathfrak{D}\left[\hat{S}_-\right]\rho + \frac{\gamma^*}{2}\mathfrak{D}\left[\hat{S}_z\right]\rho + \Gamma_e \mathfrak{D}\left[\hat{S}f_-\right]\rho, \quad (3.25)$$

where Γ_e is the electron spin relaxation rate and $\hat{S}f_- = |\uparrow\rangle\langle\downarrow|$ is an operator that flips a spin-down to a spin-up state.

3.4 Conclusion

In conclusion, in this chapter we have explained the quantum master model and shown how it can be used to calculate the dynamics of various QD systems such as a neutral exciton, biexciton and charged exciton. The quantum master equation includes two ingredients that are not considered in the semi-classical formalism: first, it includes the QD-field correlations, and additionally, the Lindblad formalism allows us to include other forms of dephasing such as pure dephasing and electron spin relaxation. We have shown that, in the low-power regime, the system can be described by a (semi-) classical model. Furthermore, we estimated in section 3.3 that, at low input power, the pure dephasing rate is about a tenth of the radiative dephasing rate, therefore it can be neglected. In section 3.4, we have shown how to extend the Jaynes–Cummings Hamiltonian in the quantum regime for more complicated level structures.